Journal of Magnetic Resonance 204 (2010) 266–272

Contents lists available at ScienceDirect

Journal of Magnetic Resonance

journal homepage: www.elsevier.com/locate/jmr

'Snap-shot' velocity vector mapping using echo-planar imaging

Alexander B. Tayler, Andrew J. Sederman *, Benedict Newling [1], Mick D. Mantle, Lynn F. Gladden

Department of Chemical Engineering and Biotechnology, University of Cambridge, Pembroke Street, Cambridge CB2 3RA, United Kingdom

ARTICLE INFO

Article history:
Received 6 January 2010
Revised 5 March 2010
Available online 9 March 2010

Keywords:
MRI
Echo-planar imaging
Multiphase flow
Velocity imaging

ABSTRACT

A 'snap-shot' ultra-fast MRI velocimetry technique based upon the echo-planar imaging (EPI) pulse sequence is presented. The new technique is an extension of the GERVAIS pulse sequence previously developed by Sederman et al. (2004) and is capable of acquiring both reference and velocity encoded phase maps following a single excitation for generation of three-component velocity vectors in under 125 ms. This approach allows velocity images of systems with a dynamic, non-periodic geometry to be obtained by MRI. The technique proved to be accurate within 5% error by comparison with Poiseuille flow in a pipe and for the transverse plane flow field in a Couette cell. It was further applied to obtain the velocity field around an impeller in a stirred vessel; an unsteady yet periodic system which otherwise could only be studied by triggered acquisitions. Good agreement was evident between the present technique and triggered conventional velocity encoded pulse sequences. Finally, new experimental data attainable only by the new sequence is demonstrated as the flow field within a mobile droplet of oil is captured as it rises through a column of water. The technique promises to be highly useful in velocimetric measurements of dynamic, non-periodic systems, and in particular for the characterisation of multiphase flow systems.

1. Introduction

In phase encoded MRI velocimetry a displacement dependent phase shift is imparted to nuclear spins undergoing coherent motion for the quantification of their velocity in one direction. For a spatially resolved velocity map there is also an inherent phase shift associated with the imaging sequence, and so the measured phase is not purely a function of the velocity. The acquisition of two images is therefore necessary; each with a different degree of velocity encoding such that the velocity proportionate phase shift may be isolated for a specific pixel within the spatial image. Conventionally, this is achieved by examining the difference between two images acquired with varying velocity encoding gradient strength, although it is also possible to obtain this measurement from the phase difference between a flowing and stationary image in the same geometry. This method becomes problematic, however, when examining a system in which no stationary or periodic geometry exists. For example, much difficulty has been encountered in obtaining velocity measurements in multiphase flow systems, wherein the dynamic nature of the system geometry prevents the acquisition of accurate phase reference data. Conventional optical velocity measurement techniques are also made difficult or impossible in such systems due to the mismatch of refractive index of the different phases, or, at worst, complete optical opacity. For this reason, it is highly desirable to obtain a so-called 'snap-shot' fast MRI velocimetry technique, wherein both a phase reference map and velocity encoded data are acquired from a single excitation.

The majority of current fast MRI velocimetry techniques [1–3] combine a velocity encoding module with either the EPI [4] or RARE [5] pulse sequences. These sequences both involve the acquisition of multiple lines of $\boldsymbol{k}$-space following a single excitation, with the fundamental difference being that EPI transverses $\boldsymbol{k}$-space by employing gradient echoes while RARE uses spin-echoes. This renders RARE a much more robust technique and permits signal attenuation to be predominately controlled by T_2 rather than T_2^*. Despite this, the increased acquisition speed of EPI and its simplified phase history (compared to RARE), for images acquired from a single excitation, provide an auspicious basis for a snap-shot three-component velocity measurement technique.

EPI velocimetry was originally implemented by Firmin et al. [6], who measured a single velocity component perpendicular to the imaging plane. These measurements were further explored by Kose [7,8], who applied the technique towards the visualisation of turbulent flow in a pipe. In his subsequent work, Kose [9] acquired two perpendicular velocity components from a single excitation to yield a 2D velocity map of turbulent flow. More recently, Sederman et al. [1] extended the later work of Kose to the acquisition of 2D velocity maps containing three-component velocity vectors and

* Corresponding author. Fax: +44 1223334796.
E-mail address: ajs40@cam.ac.uk (A.J. Sederman).
[1] Permanent Address: UNB MRI Centre, Department of Physics, University of New Brunswick, Fredericton, New Brunswick, Canada NB E3B 5A3.

1090-7807/$ - see front matter © 2010 Elsevier Inc. All rights reserved.
doi:10.1016/j.jmr.2010.03.006

named the sequence Gradient Echo Rapid Velocity and Acceleration Imaging Sequence (GERVAIS). Their approach was to acquire three velocity encoded images from a single excitation using a spin-echo to refocus the remaining magnetisation prior to each imaging sequence. The velocity proportionate phase shift was isolated by comparison with a previously acquired zero-flow reference phase map. In the present work, we seek to extend GERVAIS to include the acquisition of the phase reference maps immediately prior to the velocity encoded images. In this way, a 'snap-shot' of the velocity field of a system with changing geometry is acquired; we refer to this pulse sequence as snap-shot GERVAIS (ssG).

2. Theoretical

The pulse sequence for snap-shot GERVAIS (ssG) is shown in Fig. 1. Five images (acquired from a single excitation) are required for the generation of a three-component velocity map. These are composed of two velocity unencoded images followed by those encoded in z, x and y directions. Both unencoded images are required as the phase of the spins is inverted following the 180° pulse used to form each spin-echo, which introduces an asymmetry into the accumulated phase data between odd and even echo trains (i.e. the relative phase of the second image is shifted from that of the first and third images). Thus, the two velocity unencoded images provide all the information required to isolate the phase shift due to velocity encoding in the subsequent images. In this paper we show the acquisition of five successive images to produce a three-component velocity map, though the acquisition is not restricted to three velocity encoded images, and multiple images may be acquired for either a single or multiple components.

ssG is fundamentally similar to GERVAIS; using a train of M-BEST (or blipped) EPI [10] imaging sequences preceded by a velocity encoding module (where appropriate) and separated by 180° refocusing r.f. pulses. GERVAIS acquisitions are, however, dependent upon the velocity encoding gradients (absent in the first two scans in ssG) to spoil residual transverse magnetisation remaining from the 180° pulse due to imperfect B_1 homogeneity. To counter this, a flow compensated homospoil is included in ssG in all three directions around each 180° pulse, simultaneous to the velocity gradients, to ensure that no coherent magnetisation is present at the start of each subsequent scan. The ratio of the amplitudes of lobes of this spoiler (−1:3:2 sequentially) and a short delay between the first two lobes were determined such that the zeroth and first moments of the gradient waveform were zero immediately following the homospoil. Note that it has been experimentally verified that the simultaneous application of the homospoil and velocity gradients do not interfere with each other.

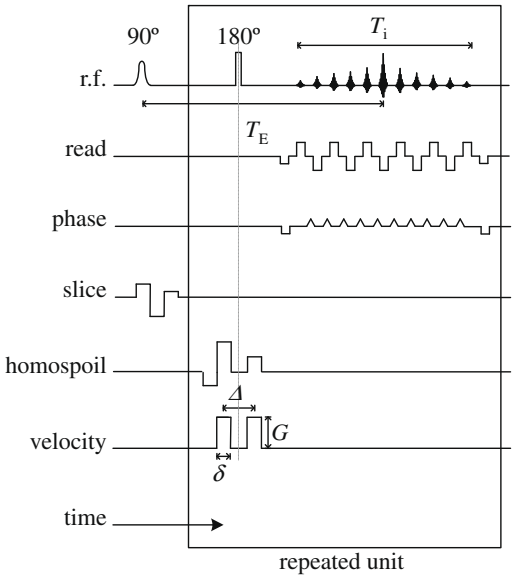

Fig. 1. Snap-shot GERVAIS pulse sequence. T_E = 24.8 ms, T_i = 18.9 ms, δ = 1.08 ms, Δ = 2.35 ms, G = 0 in first two scans, and set to maximise phase shift within a 2π window for each scan thereafter. G is typically applied in three orthogonal directions in the 3rd, 4th and 5th images.

The velocity dependent phase shift may be isolated from phase information used in imaging by considering the phase accumulation as the sequence progresses, whilst remembering that the existing phase is inverted following every 180° pulse. It is important to note that, in practise, due to gradient imperfections the region of $\boldsymbol{k}$-space sampled will shift slightly from image to image, which introduces significant phase shifts. As long as the gradient imperfections remain consistent, however, the phase accrued due to the imaging sequence will be identical for odd and even groups of spin-echoes. Thus, if we apply gradients in the z, x and y directions for the 3rd, 4th and 5th images, respectively, and consider only the scalar phase aspect of the sampled complex data:

$$\phi_1 = \phi_{\text{odd}}$$
$$\phi_2 = \phi_{\text{even}}$$
$$\phi_3 = \phi_z + \phi_{\text{odd}}$$
$$\phi_4 = \phi_x - \phi_z + \phi_{\text{even}}$$
$$\phi_5 = \phi_y - \phi_x + \phi_z + \phi_{\text{odd}}$$

where ϕ_n (where n = 1–5 for the acquisition of three-component velocity vectors) is the cumulative phase shift of the nth image, ϕ_{odd} and ϕ_{even} are the phase imparted during acquisition of odd and even images, respectively, and $\phi_{x,y,z}$ is the velocity dependent phase shift. That is:

$$\phi_z = \phi_3 - \phi_1$$
$$\phi_x = \phi_4 + \phi_3 - \phi_2 - \phi_1$$
$$\phi_y = \phi_5 + \phi_4 - \phi_2 - \phi_1$$

These phase shifts are each proportional to the magnitude of a velocity vector, the direction of which is determined by the applied velocity encoding gradient. The linear velocity in each direction is given by:

$$v_i = \frac{\phi_i}{2\pi G_i \gamma \delta \Delta}$$

where i represents the examined direction (x, y or z), G is the velocity encoding gradient strength, γ is the gyromagnetic ratio, δ is the velocity encoding time and Δ is the observation time, as shown in Fig. 1.

3. Experimental

The technique was first applied to a stagnant water phantom, 26 mm in diameter, to verify that no unquantifiable phase shift was occurring for a static (excepting diffusion) system. In order to demonstrate quantitivity in the axial direction, ssG was then applied to the measurement of fully-developed laminar flow in a 2 m long, 10 mm diameter Perspex (poly(methyl methacrylate), PMMA) tube. The Reynolds number in these experiments was 300 (corresponding to a mean fluid velocity of 3 cm s^{-1}). To ensure the results produced are quantitative in the transverse plane, ssG was also applied to flow in a 19 mm inner diameter, 26 mm outer diameter polyetheretherketone (PEEK) Couette cell rotating at 36 rpm (equivalent to a fluid velocity at the inner wall of 0.57 cm s^{-1} assuming a no-slip boundary condition). To demonstrate the applicability of the present technique to dynamic systems, MRI velocity images were acquired of flow around a PEEK

impeller in a 26 mm diameter mixing cell. Triggered velocity encoded single spin-echo [11] (i.e. time averaged measurements) and standard GERVAIS [1] images were also acquired of this system for comparison. Finally, velocity images were acquired of approximately 10 mm diameter droplets of decane rising through stagnant distilled water in a 12 mm diameter column. These experiments included an additional water-suppressive 1.9 ms Gaussian soft pulse, offset by a frequency of 2.8 ppm relative to the oil resonance as a precursor to the sequence shown in Fig. 1. Droplets were injected using a syringe pump (Harvard Apparatus 22) connected to a 5 mm diameter glass pipette. The shape oscillations of these droplets were recorded outside of the magnet by highspeed photography using a Photron SA-3 imaging system operating at 2000 frames per second.

The acquisition parameters for each of the experiments described above are summarised in Table 1. The experiments on the static tube of water, Couette cell and impeller systems were performed on a Bruker DMX-200 super wide-bore spectrometer at a ^{1}H frequency of 199.7 MHz, and using a 0.139 T m^{-1} three-axis shielded gradient system and 64 mm diameter birdcage coil. The Poiseuille flow and oil droplet experiments were carried out on a Bruker AV-400 spectrometer, operating at a ^{1}H frequency of 400.25 MHz. A 25 mm diameter birdcage coil was used to transmit and receive r.f. and a 1.460 T m^{-1} three-axis shielded gradient system was employed for spatial resolution and velocity encoding. For all experiments the flow encoding time (δ) was 1.08 ms and the observation time (Δ) 2.35 ms. The key timings for ssG, as shown in Fig. 1, were as follows: echo time (T_E) of 24.8 ms and imaging time (T_i) of 18.9 ms, leading to a the total acquisition time of approximately 125 ms for acquisition of the five images necessary to characterise a 3D velocity vector map.

In the application of ssG it must be kept in mind that as it is a technique based upon EPI a homogenous B_0 field is a necessity. In the observation of multiphase systems, disparity in magnetic susceptibility can be a significant source of B_0 heterogeneity that is difficult to counter by shimming due to the dynamic nature of the system geometry. Whilst this was not greatly problematic in the present experiments (as decane has a magnetic susceptibility similar to that of water) in applying ssG to other systems it may be necessary to dope the examined solutions with paramagnetic salts in order to match the magnetic susceptibility between each phase. Such techniques for magnetic susceptibility matching are prevalent in the literature (see, for example, the work of Stoll and Majors [12]).

4. Results and discussion

As a control experiment, ssG was applied to a reference sample consisting of a 30 mm diameter tube of stagnant water. Despite the absence of flow, substantial zero and first order phase shifts were present in the velocity encoded images, as shown in Fig. 2. The magnitude of these phase shifts was noted to be proportional to the strength of the magnetic field gradients used for velocity encoding, which indicates that eddy currents generated by these gradients are responsible. This observation highlights the principle weakness of ssG: by now obtaining phase reference data without velocity encoding present, eddy currents induced by the velocity encoding gradients remain unaccounted for. This is in direct contrast to GERVAIS, where the phase reference data is acquired from scans exposed to identical magnetic field gradients as those experienced by the velocity encoded scans. This artefact may be corrected by including stationary fluid around the region of interest to act as a reference zone fluid by which phase shift due to eddy currents can be quantified and eliminated. For example, by attaching NMR tubes of the fluid under observation to the outside of the examined cell, an eddy-induced phase map may be generated and subtracted from the region of interest, as demonstrated in Fig. 2. As it is evident that the eddy-induced phase shifts vary linearly across a sample, a phase correction map may be created by linear interpolation between each of the stationary phase reference points. In this case, a minimum of three phase reference points are required to generate a phase-correction plane, however four were included to ensure that a linear phase correction map was sufficient to entirely correct the artefact. It is convenient to note that for a cylindrical sample, these reference points may be placed in the 'corners' of the imaging region, such as to not impose upon the minimum achievable field-of-view. It is likely that the application of this procedure will only be necessary for the examination of low flow-rates where large velocity encoding gradients are required. It is clear from Fig. 2 that the proposed scheme was successful in correcting the artefact, with a final mean deviation from the expected phase shift of zero of less than 1.5% in all images. The correction process was similarly successful when applied to images velocity encoded in x and y directions.

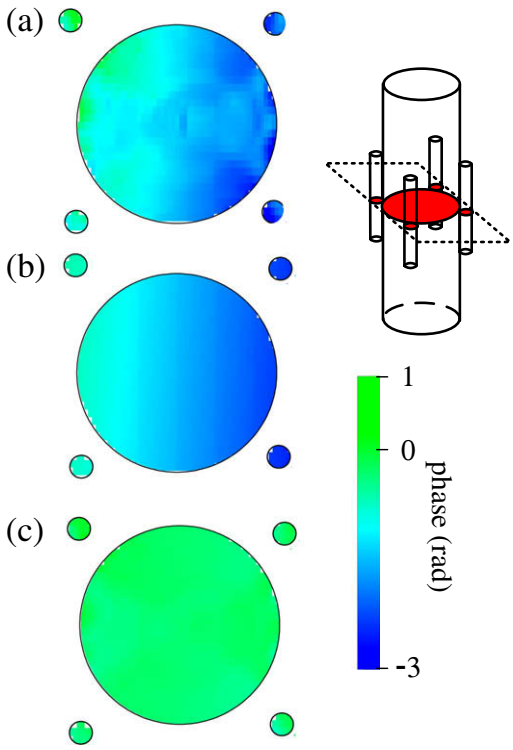

Fig. 2. (a) Effect of eddy-current induced phase shift upon a stagnant water phantom for G_z = 0.56 T m^{-1}, (b) phase-correction plane generated from stationary phase reference points and (c) corrected image.

Table 1
Experimental details.

Experiment	Spectral width (kHz)	Field-of-view (mm)	Resolution (μm)	Velocity encoding gradient strength (T m^{-1})
Static phantom	175	30 × 30	469 × 938	0.0695
Poiseuille flow	200	15 × 15	234 × 469	0.2920
Couette flow	175	30 × 30	469 × 938	0.0556
Mixing cell	175	30 × 30	469 × 938	0.0556
Rising oil drop	500	15 × 15	117 × 234	0.2920

4.1. Validation against fluid mechanics for simple systems

In order to demonstrate that quantitative velocity information is being produced from ssG it was applied to the measurement of

laminar flow in a pipe and tangential flow in a Couette cell. Solutions to the Navier–Stokes equations may be readily obtained for laminar flow in a pipe and Couette flow of a Newtonian fluid. For laminar pipe flow there ought to be no transverse plane velocity component, and the axial flow profile will be described by the Hagen–Poiseuille equation. That is, a parabolic velocity profile must be present as described by:

$$v_r = v_{\max}\left(1 - \frac{r^2}{a^2}\right)$$

where $v_{\max}$ is the maximum velocity in the pipe (twice the average velocity in the pipe, which can be estimated gravimetrically), r is radial position and a is the radius of the pipe. For flow in a Couette cell with a stationary outer wall and a marker fluid in the inner cylinder, the tangential velocity profile in the cell is given by:

$$v_\theta = \omega r \quad 0 < r < R_1$$
$$v_\theta = \frac{\omega R_1^2}{r}\frac{(R_2^2 - r^2)}{(R_2^2 - R_1^2)} \quad R_1 \leqslant r < R_2$$

where ω is the frequency of rotation of the inner cylinder and R_1 and R_2 are the inner and outer radii of the cell geometry. Fig. 3 shows a comparison of flow profiles for laminar and Couette flow with the theory.

It is evident from this comparison that very good agreement exists between the new experimental technique and the theory, with the non-zero wall velocities likely due to partial volume effects. As expected, no velocity component was apparent in the transverse plane for laminar flow. The Couette flow profile also behaved as expected, with rotationally symmetrical tangential flow patterns being produced, and no longitudinal flow (Taylor vortices are not expected for such low rotation rates). We noticed that the eddy-phase effect, described above, was present in the Couette cell images, which necessitated the use of phase reference points. The higher noise level present in the Couette cell profile relative to the laminar flow data is most likely due to the increased T_2 weighting of the later images acquired in the series. The eddy-phase effect was not apparent for the laminar flow image due to the higher coherent flow velocities present in this system permitting the use of weaker velocity gradients. This suggests that the eddy-phase artefact may be reduced by increasing the velocity encoding (δ) and observation (Δ) times, while keeping $\delta\Delta G$ constant, within the constraints imposed by the relaxation of the magnetisation and the time scales of the fluid phenomena under observation. The mean error (relative to the analytical result) for the laminar flow experiments was 3.5% and 5.6% for the Couette cell profile: both within the 5–10% accuracy range of EPI velocimetry previously established [13].

4.2. Velocity imaging of a mixing cell with impeller

The principle advantage of ssG is its ability to rapidly capture velocity fields in situations where acquiring a separate reference phase map is impractical or impossible. For example, attempting to visualise the velocity field in a stirred cell is difficult due to the moving geometry of the system associated with the rotating impeller. Moser et al. [14] demonstrated that it is possible to acquire velocity encoded images for a given impeller position by synchronising the acquisition with the impeller rotation. This approach, however, requires a perfectly periodic system and may not always be practical to implement. Rather, it is substantially more straightforward to image this system using a snap-shot technique.

To illustrate this point, ssG images were acquired of a 3 cm diameter mixing cell, stirred by an impeller rotating at 36 rpm. For the removal of the eddy-phase artefact, four NMR tubes filled with water were attached to the outside of the vessel. Additionally, optically triggered velocity encoded single spin-echo and GERVAIS images were acquired to demonstrate that the new technique is consistent with conventional MRI velocimetry. A comparison between three images acquired in this manner is provided in Fig. 4. From comparison of these images it is evident that the snap-shot technique has successfully captured all the major features of the flow field around the impeller. In the longitudinal direction, fluid is observed to flow down between the impeller blades and circulate back up at the sides of the vessel. In the transverse plane, the fluid between the blades flows at a speed approximately equivalent to that of the impeller rotation while dropping off to zero at the vessel walls. Like the GERVAIS image, ssG highlights the somewhat asymmetrical nature of the flow in the cell. From repeat images using both triggered GERVAIS and ssG it is evident that there is a chaotic element to the flow in the mixing cell, which is responsible for minor deviations from the mean flow field. These temporally local features are not apparent in the time averaged, triggered spin-echo velocity image. As expected, ssG is somewhat noisier than the other two techniques, which is largely due to the increased T_2^*-weighting of the sequence.

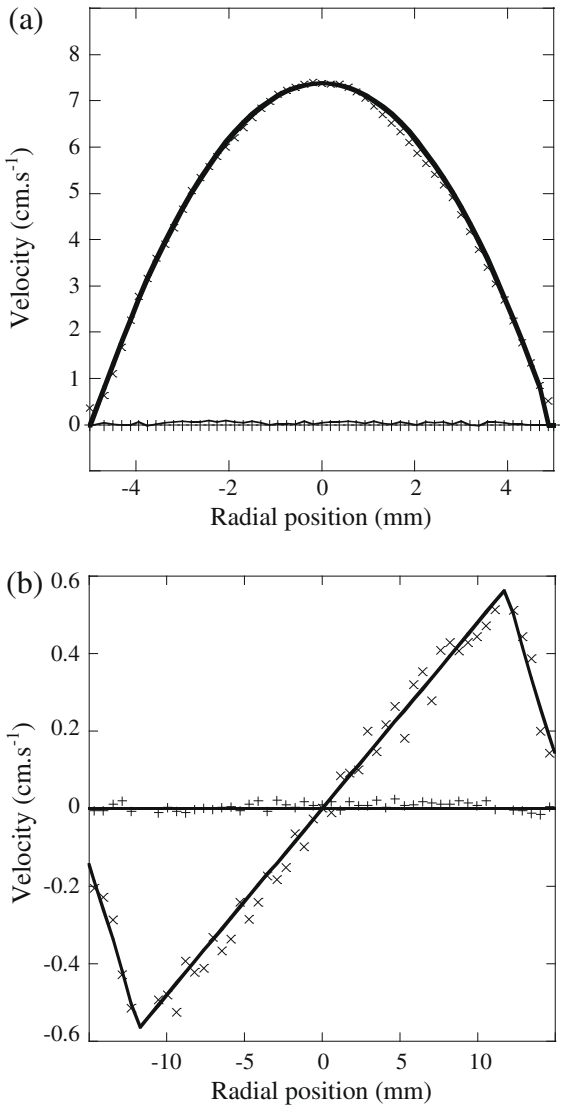

Fig. 3. Comparison of measurements obtained using ssG with fluid dynamics theory (line) for: (a) laminar flow in a pipe (× longitudinal flow, + transverse flow) and (b) Couette flow with marker fluid present (× tangential flow, + longitudinal flow).

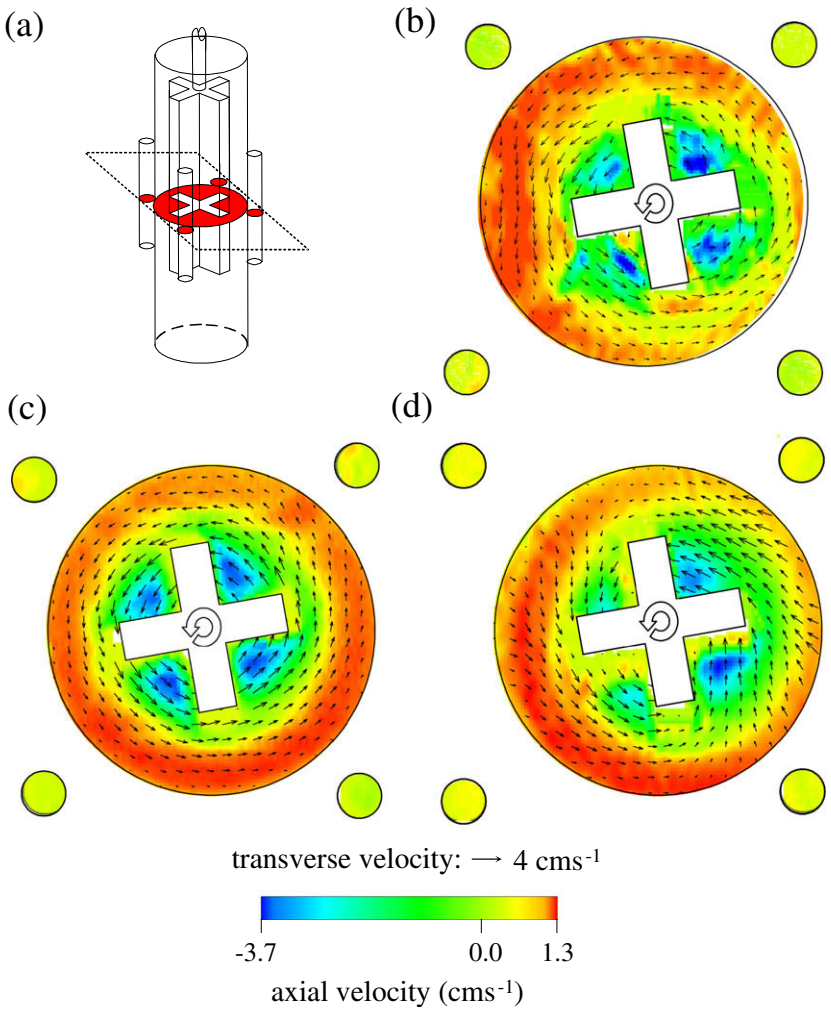

Fig. 4. Comparison of velocity images for an impeller rotating at 36 rpm in a mixing cell with stationary phase reference points included showing: (a) a schematic of the system, (b) velocity image acquired with ssG, (c) a triggered velocity encoded single spin-echo acquisition and (d) a triggered standard GERVAIS image of the same system. Note that only every second velocity vector in the transverse plane has been shown here for the sake of clarity.

4.3. Flow field within a rising oil drop

Rapidly changing systems which do not exhibit such convenient periodicity as a stirred tank become effectively impossible to obtain velocity images for using conventional MRI velocimetry. Here we consider an oil-droplet rising through a column of water under its own buoyancy. Characterising the internal flow field of such a droplet is of great interest in the design of liquid–liquid mass transfer units, as is evidenced by the observation that the analytical solution of Kronig and Brink [15] for Stokes-type recirculation within a droplet is known to greatly underestimate the rate of droplet-side mass transfer. Amar et al. [16] have recently presented MRI velocity measurements on the internal flow vortices of an oil-drop held static in a contraction against a downward flow. These measurements are, however, limited to a flow-rate such that buoyancy and drag forces acting on the droplet are balanced. Further, large, deformed droplets ($Re > 100$) undergo shape oscillations and path deviations as they rise (known as secondary motion [17]), which are also neglected in observations of a static droplet. The application of ssG allows the velocity field within a mobile and dynamic oil droplet to be observed by MRI for the first time. Fig. 5 shows example images of this type for approximately 10 mm cross-sectional diameter droplets of decane as they rise through stagnant distilled water. Whilst some element of the expected rotational flow is present, the flow field inside the droplet is asymmetrical. It is important to note here that the droplets were undergoing significant shape deformation and path instability, as captured by highspeed photography with the column removed from the magnet. Shape contours extracted from these photographs are shown in Fig. 5c) and a highspeed video is available as online Supplementary data. The velocity images imply an intimate coupling between the internal flow field of the droplet and its secondary motion, and suggest that the shape oscillations of a rising drop may be the dominant factor in determining the internal velocity field. These results also provide clues regarding the mechanism of droplet shape oscillation. In particular, the symmetry in the transverse plane flow field about a diagonal line in Fig. 5a) suggests that the droplet is deforming about this axis in a manner congruent with the capillary wave model for bubble shape oscillations proposed by Lunde and Perkins [18]. It is also of interest that the axial flow field demonstrates some symmetry about the opposite diagonal in both droplets. The net axial velocity of the droplet measured from the velocity images in Fig. 5 is 9.48 cm s^{-1}. This is in excellent agreement with the droplet rise velocity extracted from the highspeed photography data, of 9.45 cm s^{-1}. Similar checks cannot be made in the transverse plane, as only a slice of the droplet has been excited, and thus the transverse vectors need not necessarily sum to zero. This rise rate is equivalent to a shift of 1.2 cm

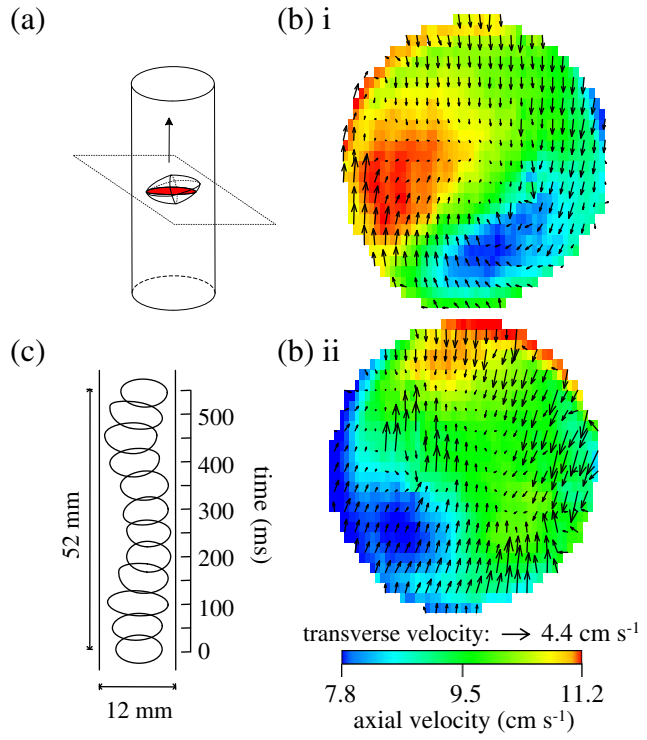

Fig. 5. (a) Schematic of system highlighting the plane being imaged, (b) ssG images of the internal flow field of two droplets (i and ii) of decane captured as the drops rose through a column of distilled water. Note that the signal from the water in these images has been suppressed and (c) Droplet shape contours extracted from highspeed photography. Highspeed video is available online as Supplementary data.

over the course of the acquisition period. Spatial averaging over this length is, however, minimised as the data produced by ssG are effectively Lagrangian (i.e. only spins disturbed from equilibrium in the original slice-selective excitation emit a signal for the duration of the pulse sequence, irrespective of where in the r.f. coil they are transported to). While the displacements in the transverse plane are less than those in the slice direction, some degree of spatial averaging in the imaging plane must be accepted.

ssG overcomes some of the limitations of standard implementations of EPI for velocity measurement in chaotic systems. In particular, EPI is known to exhibit spatially local signal attenuation in the presence of excessive fluid shear [19]. This is partially because the train of phase increment blips used for imaging is not velocity compensated, and thus, in the presence of high fluid velocities, phase shifts will be introduced that can compromise image integrity and contribute to the first gradient moment, thereby introducing error into the calculation of fluid velocity. This problem can be addressed by velocity compensating each phase blip, which substantially increases imaging time, or by limiting the application of EPI and EPI-based velocimetric techniques to systems exhibiting relatively low velocities in the phase direction. In these cases the phase shift due to velocity encoding in the imaging sequence is much less than the phase encodings applied for velocity measurement. For faster flows, by acquiring phase reference data in the presence of similar fluid velocities to those present in the velocity encoded scans, the velocity encoding associated with the imaging phase gradient is removed when the imaging phase is subtracted. While this can be achieved for steady state or periodic systems by acquisition of two separate images using an increment in the velocity encoding gradient, only ssG permits the acquisition of reference and velocity encoded data in close enough succession for the same to apply to chaotic systems. Thus, ssG reduces the consequences of applying a non-velocity compensated imaging sequence to unsteady, non-periodic flowing systems, thereby enabling the measurement of higher transient velocities than those previously attainable.

Examples of other dynamic systems which may now be examined, for the first time, by fast MRI velocimetry include: droplet formation, break-up and coalescence; unsteady climbing flows and falling films; bubbly flows and particle settling. In applications beyond those in the physical sciences, EPI velocimetry has been employed in breath-hold and synchronised acquisitions for the study of blood flow in the human body [20,21]. The present technique, however, may be able to broaden the scope of such studies; allowing for patient motion or other irregularities. In fact, the present technique permits the application of MRI velocimetry to any unsteady system which changes at a rate slowly enough that spatial blurring is acceptable within the 125 ms acquisition time.

5. Conclusions

A snap-shot, three-component MRI velocimetry technique based upon the EPI imaging sequence was developed and validated against the theory for laminar flow in a pipe and a Couette cell. Three-component velocity images were obtained in approximately 125 ms, rendering the technique suitable for application to systems that change at a rate slow enough for acceptable spatial blurring over this period. ssG was firstly demonstrated on a dynamic yet periodic system for validation against standard MRI velocimetric techniques. Velocity fields were measured around a rotating impeller, and compared with triggered acquisition velocity encoded spin-echo and GERVAIS images of the same system. Whilst good agreement between the measurement techniques was evident, the one shot technique was substantially less complicated to implement. For slow flows that required high velocity encoding gradients, eddy currents can be a source of significant error for the ssG technique as the phase reference maps are exposed to different magnetic field gradients than those experienced by the velocity encoded images (this is in contrast to GERVAIS, where the effects of eddy currents are minimised by identical gradient application for the flowing and non-flowing images). The effect of eddy currents was minimised by acquiring phase reference points surrounding the region of interest. These reference points allowed the generation of an eddy-induced phase correction map. This procedure, however, was only necessary for the examination of low velocities, in our case less than 2 cm s^{-1}, due to the relatively high strength velocity encoding gradients required for velocity resolution in this range. New experimental data for the flow field within a rising droplet of decane were also presented. These snap-shot images of a mobile droplet are the first of their type existing in the literature and demonstrate the great potential of ssG for the velocimetric characterisation of multiphase flow systems.

Acknowledgments

The authors wish to thank the EPSRC for financial support under the Grants GR/S20789/01, EP/G547241/1 and EP/F047991/1. They also thank the EPSRC equipment pool for the loan of a high-speed camera. BN would like to thank NSERC of Canada and the Harrison McCain Foundation for a Visitorship Award. ABT would like to express his sincere gratitude to the Cambridge Commonwealth Trust and Trinity College, Cambridge for provision of a studentship.

Appendix A. Supplementary data

Supplementary data associated with this article can be found, in the online version, at doi:10.1016/j.jmr.2010.03.006.

References

[1] A.J. Sederman, M.D. Mantle, C. Buckley, L.F. Gladden, MRI technique for measurement of velocity vectors, acceleration, and autocorrelation functions in turbulent flow, J. Magn. Reson. 166 (2004) 182–189.

[2] S. Ahola, J. Perlo, F. Casanova, S. Stapf, B. Blumich, Multiecho sequence for velocity imaging in inhomogeneous rf fields, J. Magn. Reson. (2006) 143–151.

[3] P. Galvosas, P.T. Callaghan, Fast magnetic resonance imaging and velocimetry for liquids under high flow rates, J. Magn. Reson. (2006) 119–125.

[4] P. Mansfield, Multi-planar image formation using NMR spin echoes, J. Phys. C 10 (1977) L55–L58.

[5] J. Hennig, A. Nauerth, H. Friedburg, RARE imaging: a fast imaging method for clinical MR, Magn. Reson. Med. 3 (1986) 823–833.

[6] D.N. Firmin, R.H. Klipstein, G.L. Hounsfield, M.P. Paley, D.B. Longmore, Echo-planar high-resolution flow velocity mapping, Magn. Reson. Med. 12 (1989) 316–327.

[7] K. Kose, NMR imaging of turbulent structure in a transitional pipe flow, J. Phys. D. 23 (1990) 981–983.

[8] K. Kose, Instantaneous flow-distribution measurements of the equilibrium turbulent region in a circular pipe using ultrafast NMR imaging, Phys. Rev. A 44 (1991) 2495–2504.

[9] K. Kose, One-shot velocity mapping using multiple spin-echo EPI and its application to turbulent flow, J. Magn. Reson. 92 (1991) 631–635.

[10] A.M. Howseman, M.K. Stehlingm, B. Chapman, R. Coxon, R. Turner, R.J. Ordidge, M.G. Cawley, P. Glover, P. Mansfield, R.E. Coupland, Improvements in snap-shot nuclear magnetic resonance imaging, Brit. J. Radiol. 61 (1988) 822–828.

[11] R. Stevenson, S.T.L. Harrison, M.D. Mantle, A.J. Sederman, T.L. Moraczewski, M.L. Johns, Analysis of partial suspension in stirred mixing cells using both MRI and ERT, Chem. Eng. Sci. 65 (2010) 1385–1393.

[12] M.E. Stoll, T.J. Majors, Reduction of magnetic susceptibility broadening in NMR by susceptibility matching, J. Magn. Reson 46 (1982) 283–288.

[13] K.W. Moser, J.G. Georgiadis, R.O. Buckius, On the accuracy of EPI-based phase contrast velocimetry, Magn. Reson. Imaging 18 (2000) 1115–1123.

[14] K.W. Moser, L.G. Raguin, J.G. Georgiadis, Synchronized EPI phase contrast velocimetry in a mixing reactor, Magn. Reson. Imaging 21 (2003) 127–133.

[15] R. Kronig, J.C. Brink, On the theory of extraction from falling droplets, Appl. Sci. Res. A2 (1951) 142–154.

[16] A. Amar, E. Groß-Hardt, A.A. Khrapitchev, S. Stapf, A. Pfennig, B. Blumich, Visualizing flow vortices inside a single levitated drop, J. Magn. Reson. 177 (2005) 74–85.

[17] R. Clift, J.R. Grace, M.E. Weber, Bubbles, Drops, and Particles, Academic press, New York, 1978.

[18] K. Lunde, R.J. Perkins, Shape oscillations of rising bubbles, Appl. Sci. Res. 58 (1998) 208–387.

[19] J.C. Gatenby, J.C. Gore, Echo-planar-imaging studies of turbulent flow, J. Magn. Reson. Series A 121 (1996) 193–200.

[20] P.D. Gatehouse, D.N. Firmin, S. Collins, D.B. Lonmore, Real time blood flow imaging by spiral scan phase velocity mapping, Magn. Reson. Med. 31 (1994) 504–512.

[21] G.B. Pike, C.H. Meyer, T.J. Brosnan, N.J. Pelc, Magnetic resonance velocity imaging using a fast spiral phase contrast sequence, Magn. Reson. Med. 32 (1994) 476–483.